Quasielastic Lepton Scattering off Two-Component Dark Matter in Hypercolor Model

Vitaly Beylin [1],* , **Maxim Bezuglov** [2,3], **Vladimir Kuksa** [1] **and Egor Tretiakov** [2,3]

[1] Institute of Physics, Southern Federal University, Stachki 194, 344090 Rostov on Don, Russia; vkuksa47@mail.ru

[2] Bogoliubov Laboratory of Theoretical Physics, Joint Institute for Nuclear Research, Joliot-Curie 6, 141980 Dubna, Russia; bezuglov.ma@phystech.edu (M.B.); tretiakov.ea@phystech.edu (E.T.)

[3] Moscow Institute of Physics and Technology Institute str. 7, 141701 Dolgoprudny, Moscow Region, Russia

* Correspondence: vitbeylin@gmail.com

Abstract: The interaction of high-energy leptons with components of Dark Matter in a hypercolor model is considered. The possibility of detection, using IceCube secondary neutrinos produced by quasielastic scattering of cosmic ray electrons off hidden mass particles, is investigated. The dominant contribution to the cross section results from diagrams with scalar exchanges. A strong dependence of the total cross section on the Dark Matter components mass is also found.

1. Introduction

In the energy region of the order of several TeV, collider studies do not give a clear answer to the question of the nature of phenomena beyond the Standard Model (SM). Some puzzles appear in experimental data, however, they are quickly solved with an increase in the statistics and accuracy of experiments (as in the history with two-photon peak at 750 GeV, for example). In all such cases, we do not have a clear understanding of how to establish the Standard Model (SM) extension type. The promising ideas of supersymmetry turned out to be pushed back to the high-energy region, and are unavailable for detailed verification up to now. When lacking data in the accessible energy range, indirect research methods relying on astrophysical measurements and observations are of particular importance. In other words, now we shift our focus to those experiments posed by Nature itself. We analyze data on cosmic rays, gravitational waves, photons and neutrino originating from galactic and extragalactic sources which are gathered by cosmic telescopes and ground observatories (like IceCube, Antares, LIGO, or LHAASO in the near future). Then, the measured spectra of particles and waves are interpreted in terms of scenarios of the SM extended. Beyond the SM, new types of particles arise from more general groups of symmetry together with a lot of unknown parameters: masses, couplings, angles of mixing, etc. Some of them can be fixed in a reasonable intervals of values due to experimental constraints for electroweak (EW) data (particularly, for Peskin-Tackeuchi parameters), Dark Matter (DM) relic abundance and so on. It is important to explore indirect methods of studying the high-energy phenomena beyond the SM [1–7].

The origin and characteristics of the hidden mass carriers are an important probe and a generic attribute of the SM extension type. Various DM candidates generate different signals that can be used to discriminate the models. In particular, these are annihilation spectra of photons and/or leptons. Simultaneously, we can check model profiles of the DM in the Galaxy and consider the possibility of the DM clumpiness [8]. Note, there is a chance to analyze manifestations of the hidden mass by

studying of cosmic rays scattering off the DM particles. It can be an important probe to study the DM space distribution in dependence on symmetry of the model and its specific properties and parameters.

Quasielastic scattering of cosmic electrons and/or neutrino off hidden mass components was considered in the minimal model of vectorlike hypercolor [9–17]. See also other minimal scenarios in Refs. [18,19]. This paper continues our studies in [20,21]. There, quasielastic scattering of cosmic electrons off hyperpion component of hidden mass was studied and also there were presented some initial approvals and preliminary results of analysis of high-energy electrons interaction with hyperbaryon component. Here, we will discuss the scattering processes in more detail.

In Section 2 we present the main statements of the hypercolor $SU(4) \rightarrow Sp(4)$ model and remind some input parameters which are necessary for the analysis. Section 3 is devoted to results for the electron scattering of the DM components. In the Section 4 an estimation of neutrino observation possibility is done. Some important features of these type processes can be found in the Conclusions and Discussions section.

2. The Vectorlike Hypercolor Model

The ideology of hypercolor models is originated from Technicolor, here, a similar addition of several (heavy) fermions to the SM occurs [22–25]. The new fields transform under some symmetry group and interact with standard gauge bosons through vector currents after transition to Dirac doublets from left doublets of hyperquarks (H-quarks) [9,10]. In the minimal scenario we operate with two generations ($A = 1, 2$) of left-handed two-color H-quarks, whose bi-doublet can be written as a matrix $Q_{L(A)}^{a\underline{a}}$, here $a = 1, 2$ and $\underline{a} = 1, 2$ are indices of $SU(2)_L$ and $SU(2)_{HC}$ fundamental representations respectively. In formulas below, the hypercolor group indices are underlined.

Under $U(1)_Y \otimes SU(2)_L \otimes SU(2)_{HC}$ this bi-doublet transforms as

$$(Q_{L(A)}^{a\underline{a}})' = Q_{L(A)}^{a\underline{a}} + ig_B Y_A \theta Q_{L(A)}^{a\underline{a}} + \frac{i}{2} g_W \theta_k \tau_k^{ab} Q_{L(A)}^{b\underline{a}} + \frac{i}{2} g_{HC} \varphi_{\underline{k}} \tau_{\underline{k}}^{\underline{ab}} Q_{L(A)}^{a\underline{b}}. \tag{1}$$

Here $Q_{L(A)}^{1\underline{a}} = U_{L(A)}^{\underline{a}}$, $Q_{L(A)}^{2\underline{a}} = D_{L(A)}^{\underline{a}}$, the H-quarks charges, $q_{U,D}$, are fixed by an arbitrary hypercharges Y_A. The right-handed singlets (with respect to electroweak $SU(2)_L$ group) are transformed as follows:

$$(S_{R(A)}^{\underline{a}})' = S_{R(A)}^{\underline{a}} + ig_B Y_{R(A)} \theta S_{R(A)}^{\underline{a}} + \frac{i}{2} g_{HC} \varphi_{\underline{k}} \tau_{\underline{k}}^{\underline{ab}} S_{R(A)}^{\underline{b}}, \tag{2}$$

where $A = 1, 2$ and $Y_{R(A)}$ are hypercharges of singlets. Keeping the first generation unchanged, the second generation fields undergo charge conjugation operation, $\hat{\mathbf{C}}$, which obviously changes the fermion chirality:

$$Q_{L(2)}^{Ca\underline{a}} = \hat{\mathbf{C}} Q_{L(2)}^{a\underline{a}}. \tag{3}$$

The charge conjugated fields are transformed as

$$(Q_{L(2)}^{Ca\underline{a}})' = Q_{L(2)}^{Ca\underline{a}} - ig_B Y_2 Q_{L(2)}^{Ca\underline{a}} - \frac{i}{2} g_W \theta_k (\tau_k^{ab})^* Q_{L(2)}^{Cb\underline{a}} - \frac{i}{2} g_{HC} \varphi_{\underline{k}} (\tau_{\underline{k}}^{\underline{ab}})^* Q_{L(2)}^{Ca\underline{b}}. \tag{4}$$

Now, the H-quark fields are redefined in a following manner:

$$Q_{R(2)}^{a\underline{a}} = \epsilon^{ab} \epsilon^{\underline{ab}} Q_{L(2)}^{Cb\underline{b}}, \quad \epsilon^{ab} = i\sigma_2^{ab}. \tag{5}$$

Multiplying both sides of (4) by $\epsilon^{ab} \epsilon^{\underline{ab}}$ and using the following properties of $SU(2)$ group matrices

$$\epsilon^{ac} \epsilon^{bc} = \delta^{ab}, \quad \epsilon^{ab} = -\epsilon^{ba}, \quad \epsilon^{ab} (\tau_k^{bc})^* \epsilon^{cf} = \tau_k^{af}, \tag{6}$$

we get:

$$(Q_{R(2)}^{a\underline{a}})' = Q_{R(2)}^{a\underline{a}} - ig_B Y_2 Q_{R(2)}^{a\underline{a}} + \frac{i}{2} g_W \theta_k \tau_k^{ab} Q_{R(2)}^{b\underline{a}} + \frac{i}{2} g_{HC} \varphi_{\underline{k}} \tau_{\underline{k}}^{\underline{ab}} Q_{R(2)}^{a\underline{b}}. \tag{7}$$

This transformation law coincides with the one given by Formula (1) for the first generation ($A = 1$) when $Y_2 = -Y_1$.

Therefore, the right-handed partner of the first generation is constructed with the help of left-handed fields of the second generation in two steps: charge conjugation and redefinition. Combining these fields, we come to Dirac state:

$$Q^{a\underline{a}} = Q_{L(1)}^{a\underline{a}} + Q_{R(2)}^{a\underline{a}} = Q_{L(1)}^{a\underline{a}} + \epsilon^{ab} \epsilon^{\underline{ab}} Q_{L(2)}^{Cb\underline{b}}. \tag{8}$$

Now, both left- and right-handed components of the field have the same transformation properties. It results to chirally symmetric interaction of the Dirac H-quarks with the EW vector bosons.

The right-handed field $S_{R(2)}^a$ can be also redefined:

$$S_L^a = \epsilon^{\underline{ab}} \hat{C} S_{R(2)}^b. \tag{9}$$

Then, the redefined field transforms as the right-handed singlet $S_{R(1)}$ if $Y_{R(2)} = -Y_{R(1)}$, so we get a usual Dirac mass term as the sum of left and right parts. Both current and constituent H-quark masses can be introduced because the mass term does not violate the model symmetry. The simplest way to do this is to use a singlet real scalar, s, which has a non-zero v.e.v., $s = \tilde{\sigma} + u$, where $u = \langle s \rangle$. Just interaction of the H-quarks with this scalar field provides Dirac type mass term for H-quarks. Importantly, to construct a Dirac state with the vectorlike interaction from two Weyl spinors, we should require the initial fields for the first and second families to have opposite hypercharges, $Y_1 = -Y_2$. The same requirement follows from the condition of the absence of anomalies in the model. It should be noted that the suggested construction of vectorlike interaction is valid due to unique properties of $SU(2)_{HC}$ group and for the case of an even number of generations.

Thus, the initial Lagrangian can be rearranged into a Lagrangian of Dirac H-quarks. As it was noted in Ref. [17,19], this procedure is possible for any type of techni- or hyperchromodynamics with H-quarks in selfcontragredient representation of H-confinement group. The fundamental symplectic and pseudoreal representation of $SU(2)_{HC}$ is just the most simple case. Global symmetry of the model Lagrangian is induced by rotations in the space of four initial chiral fermion fields. It is symmetry under Pauli-Gürsey group $SU(4)$, the chiral symmetry corresponds to a subgroup of the Pauli-Gürsey group. Having the mass term structure, H-quark condensate $\langle \bar{Q}Q \rangle$ results into dynamical breaking of the symmetry, $SU(4) \to Sp(4)$, and generates the mass term for H-quarks. More exactly, the global symmetry is broken both explicitly and dynamically: explicitly—by EW and Yukawa interactions and the H-quark mass terms, dynamically—by H-quark condensate [19]. Then, the broken generators of $SU(4)$ would be accompanied by a set of pseudo-Nambu-Goldstone (pNG) states with the spectrum which depends on the way of the symmetry breaking.

Note, the v.e.v. u which is proportional to $\langle \bar{Q}Q \rangle$, breaks the global symmetry $SU(4)$ spontaneously as the chiral symmetry in QCD is dynamically broken by the quark condensate $\langle \bar{q}q \rangle$. In the framework of linear sigma model [26–29], the spontaneous breaking is induced by non-zero value of v.e.v. of scalar field σ meson field. The sigma model scheme was used to introduce H-quark—H-hadron interactions in analogy with standard quark-hadron low-energy physics. It results to appearing of scalar pNG singlet, $\tilde{\sigma}$−meson, which mixes with Higgs meson, h. The angle of mixing, θ, is an important parameter of the model [17], its value is constrained by data on Peskin-Tackeuchi parameters. It has been checked that all known restrictions for the oblique corrections are fulfilled in this variant of hypercolor. Namely, parameter $T = 0$ if the hypercharge is zero and h–$\tilde{\sigma}$ mixing is absent. In the scenario with a non-zero hypercharge and mixing, to provide a necessary smallness of the T parameter and agreement with known characteristics of the SM Higgs boson, the mixing angle should be sufficiently small, $\sin \theta \ll 0.1$ [9,11,30].

Importantly, total Lagrangian of the model is invariant under residual global $U(1)_{HB}$ symmetry. It allows introducing a conserved H-baryon number, consequently, the lightest H-diquark B^0 is stable. Besides, the H-quark sector of the model Lagrangian is invariant under modified charge conjugation of the H-quark fields (hyper-*G*-parity, *HG*-parity) which is defined as follows:

$$(Q_{a\underline{a}})^{HG} = \epsilon_{ab}\epsilon_{\underline{ab}}Q_{b\underline{b}}^C. \tag{10}$$

Here C is the charge conjugation, a, b are isotopic indices, and $\underline{a}$, $\underline{b}$ are hypercolor indices. The Lagrangian invariance can be strongly proved (see Ref. [19,31] and references therein), and it results to the relation $\tilde{\pi}'_k = -\tilde{\pi}_k$. Then, $\tilde{\pi}$ is odd under modified charge conjugation, while the SM fields are even. In other words, the *HG*-parity is a good quantum number of the theory. Namely, *HG*-odd $\tilde{\pi}$ does not decay into only SM final particles. Therefore, the lightest neutral $\tilde{\pi}^0$ is stable [17,32,33].

Thus, we have the H-color model which can be reconciled with the electroweak precision constraints quite easily, since H-quarks are vectorlike. We also guess that H-quarks interact with gauge vector bosons as the fundamental ones. In sigma-model framework H-quarks can form H-mesons and/or H-baryons. The complete set of the lightest pNG states (spin-0 H-hadrons) includes—pseudoscalar H-pions $\tilde{\pi}_k$ and scalar complex H-diquarks (H-baryons) B^0,—their parity partners $\tilde{a}_k$ and A^0, and singlet H-mesons $\tilde{\sigma}$ and $\tilde{\eta}$. These pNG states are listed in Table 1 along with their quantum numbers and associated H-quark currents. There are used the following notations: T is the weak isospin. $\tilde{G}$ denotes hyper-*G*-parity of a state (see Ref. [17,31] for detail). $\tilde{B}$ is the H-baryon number. Q_{em} is the electric charge (in units of the positron charge $e = |e|$). The H-quark charges are $Q_{\text{em}}^U = (Y_Q + 1)/2$, $Q_{\text{em}}^D = (Y_Q - 1)/2$, ϵ_{ab} and $\epsilon_{\underline{ab}}$ are matrices $i\sigma_{ab}^2$ for EW and H-color groups. Note, H-baryons do not carry intrinsic *C*- and *HG*-parities, since the charge conjugation reverses the sign of the H-baryon number.

Table 1. Part of the lightest (pseudo)scalar H-hadrons and corresponding H-quark currents in $SU(2)_{HC}$ model.

State	H-Quark Current	$T^{\tilde{G}}(J^{PC})$	$\tilde{B}$	Q_{em}
σ	$\bar{Q}Q$	$0^+(0^{++})$	0	0
η	$i\bar{Q}\gamma_5 Q$	$0^+(0^{-+})$	0	0
a_k	$\bar{Q}\tau_k Q$	$1^-(0^{++})$	0	$\pm 1, 0$
π_k	$i\bar{Q}\gamma_5\tau_k Q$	$1^-(0^{-+})$	0	$\pm 1, 0$
A	$\bar{Q}^C\epsilon_{ab}\epsilon_{\underline{ab}}Q$	$0\ (0^-\ )$	1	Y_Q
B	$i\bar{Q}^C\epsilon_{ab}\epsilon_{\underline{ab}}\gamma_5 Q$	$0\ (0^+\ )$	1	Y_Q

Here, we consider only low-lying stable states as the DM components to analyze their quasielastic interaction with cosmic rays. Namely, we assume that all other degrees of freedom are much heavier and cannot be produced in these reactions. Add also that the hypercolor models are now under intensive study on the lattice, there appear papers with an analysis of spectra of hypermesons masses [34–36], particularly, of vector hyperparticles. As we supposed, from lattice calculations it also follows that they are much heavier than the stable ones.

To study the processes of scattering numerically, we will use Lagrangians of *W*- and *Z*-bosons interaction with leptons, standard light quarks, hyperquarks and hyperpions. All of them can be found in earlier papers [17,19,20,31]. Therefore, we add here only vertexes of scalar self-interactions and interactions of scalars with pNG—as it is shown, these interactions give dominant contributions to the total cross sections of the processes studied:

$$L = -\lambda_{00}h^3 \left(v + \frac{1}{4}h\right) - \frac{1}{4}\lambda_{11}\left(B_{\dot{\alpha}}B_{\dot{\alpha}} + \sigma'^2\right)\left(B_{\dot{\alpha}}B_{\dot{\alpha}} + \sigma'^2 + 4u\sigma'\right)$$
$$-\frac{1}{4}\lambda_{01}h\left[(2v + h)\left(B_{\dot{\alpha}}B_{\dot{\alpha}} + \sigma'^2\right) + 2u\sigma'h\right] - \frac{1}{4}\lambda_{02}h(2v + h)(A_{\dot{\alpha}}A_{\dot{\alpha}} + \tilde{\eta}^2)$$
$$-\frac{1}{4}\lambda_{12}\left(B_{\dot{\alpha}}B_{\dot{\alpha}} + \sigma'^2 + 2u\sigma'\right)\left(A_{\dot{\alpha}}A_{\dot{\alpha}} + \tilde{\eta}^2\right) - \frac{1}{4}\lambda_{22}(A_{\dot{\alpha}}A_{\dot{\alpha}} + \tilde{\eta}^2)^2 \qquad (11)$$
$$-\lambda_{33}\left[-(u + \sigma')\tilde{\eta} + \tilde{a}_k\tilde{\pi}_k + \bar{B}^0 A^0 + \bar{A}^0 B^0\right]^2,$$

where $A_{\dot{\alpha}}A_{\dot{\alpha}} = 2\tilde{a}^+\tilde{a}^- + \tilde{a}^0\tilde{a}^0 + 2\bar{A}^0 A^0$, $B_{\dot{\alpha}}B_{\dot{\alpha}} = 2\tilde{\pi}^+\tilde{\pi}^- + \tilde{\pi}^0\tilde{\pi}^0 + 2\bar{B}^0 B^0$.

Remind that the Peskin-Tackeuchi parameters were calculated and it was shown that the angle of mixing of scalars should be small, $\sin\theta \ll 0.1$. The mass difference for hyperpion multiplet have been found as small as $\Delta M_{\tilde{\pi}} = m_{\tilde{\pi}^\pm} - m_{\tilde{\pi}^0} \approx 0.16$ GeV [13,37]. The other mass splitting, $\Delta M_{B\tilde{\pi}} = m_{B^0} - m_{\tilde{\pi}^0}$, is defined by electroweak contributions and depends on H-pion mass and a renormalization scale. It results from substantially different genesis of these pNG states—neutral H-pion and H-baryon (see Table 1). Then, as input parameters for the calculations we should have the values of masses of both possible DM components, B-baryon and $\tilde{\pi}^0$, v.e.v. of $\tilde{\sigma}-$meson, the angle of mixing, θ, and the value of renormalization parameter, μ [20,37]. In the numerical analysis we use the reasonable choice of the scale parameter μ in a diapason 1–2 TeV resulting in the close masses for both DM components in agreement with the analysis of the DM annihilation kinetics [20].

We also should underline that this scenario is the most compact variant to add H-quarks with vectorlike interactions and with the hypercharges providing the absence of anomalies. As a result, in this minimal hypercolor model there are no necessity to introduce H-leptons to mutual canceling the anomalies or to their interpretation as the hidden mass candidates [38–43]. That is why these additional (and possible, in principle) degrees of freedom do not considered in this study.

3. Scattering of Leptons off Hypercolor DM Particles

The process $e^- \tilde{\pi}^0 \to \nu_e \tilde{\pi}^-$ and analysis of the DM component masses based on kinetic equations have been done earlier [20]. Annihilation cross sections for DM components were calculated and studied assuming the masses of stable hypercolor particles are close in the interval 0.5–1.5 TeV. Note, the cross section was considered supposing the target (DM particle) get a small portion of projectile energy i.e., intermediate $W-$boson is not very far from its mass shell and the final $\tilde{\pi}^0$ moves as slowly as the initial one. It means that secondary neutrino from W decay should have energy $\sim 10^2$ GeV or less. More details about the charged hyperpion decays can be found in Ref. [17]. Then, taking a reasonable values of the DM component masses from the kinetic equations, the cross section of the process above had been calculated. Besides, distributions of energy and angle of emission for secondary neutrino, the number of neutrino events at IceCube were also estimated [20].

In the model, direct interactions of H-baryons, B, with photons, Z- and W-bosons are absent. It seems that photons and Z-/W- bosons can interact with this DM component through H-quarks, U, D, and/or H-pion loops in 1-loop level (see Figures 1 and 2); however, we will show further that these contributions are zero.
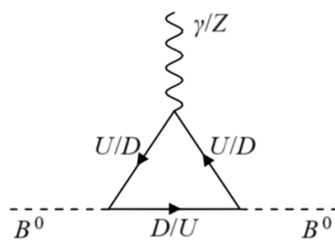

Figure 1. H-quark one-loop diagram for $BB\gamma/Z$ interaction.
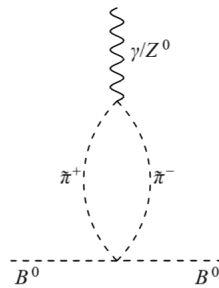
Figure 2. H-pion one-loop diagram for $BB\gamma/Z$ interaction.

To calculate this diagram, we need in the following part of the Lagrangian:

$$L = -\frac{i\kappa}{\sqrt{2}}B\bar{Q}^C_{a\alpha}\epsilon_{ab}\epsilon_{\alpha\beta}\gamma_5 Q_{b\beta} + \frac{1}{2}g_W(\bar{U}\gamma^\mu U - \bar{D}\gamma^\mu D)(c_W Z_\mu + s_W A_\mu),\tag{12}$$

where c_W and s_W—are cosine and sine of Weinberg angle; $Q_{a\alpha} = \begin{pmatrix} U_\alpha \\ D_\alpha \end{pmatrix}$ is H-quark doublet with mox $\alpha = 1, 2$; charge conjugation is define as $Q^C_{a\alpha} = \hat{C}Q_{a\alpha} = \gamma^2\gamma^0\bar{Q}_{a\alpha} = \gamma^2 Q^*_{a\alpha}$ and $\epsilon_{ab} = i\sigma_{ab} = \begin{pmatrix} 0 & 1 \\ -1 & 0. \end{pmatrix}$

To express the Lagrangian in terms of physical field of H-quarks, we use:

$$\bar{Q}^C_{a\alpha}\epsilon_{ab}\epsilon_{\alpha\beta}\gamma_5 Q_{b\beta} = U_\alpha M_{\alpha\beta}D_\beta - D_\alpha M_{\alpha\beta}U_\beta,\tag{13}$$

$M_{\alpha\beta}$ is the matrix convolving with hyperquarks U, D under spinor and hypercolor indices. Then, the amplitude has the form:

$$\Lambda^\mu \sim \int Sp\left[M\frac{\hat{q}+m}{m^2-q^2}\gamma^\mu\frac{\hat{q}+\hat{Q}+m}{m^2-(q+Q)^2}M\frac{\hat{p}_1+\hat{q}+m}{m^2-(p_1+q)^2}\right]d^4q,\tag{14}$$

here p_1, Q are external 4-momenta, M denotes $M_{\alpha\beta}$ matrix, q is 4-momentum of internal H-quark, H-quarks, U, D, are degenerated in mass). This amplitude is exactly zero as it follows from direct calculation (it is an analog of Furry's theorem in QED).

Considering interaction H-baryons with leptons through H-pion loop we use the following part of Lagrangian:

$$L = ig_W(c_W Z^\mu - s_W A^\mu)(\tilde{\pi}^-\partial_\mu\tilde{\pi}^+ - \tilde{\pi}^+\partial_\mu\tilde{\pi}^-) - 2\lambda_{11}\bar{B}^0 B^0 \tilde{\pi}^+\tilde{\pi}^-,\tag{15}$$

and the amplitude has the form:

$$\Lambda^\mu \sim \left[p^\mu\int\frac{d^4q}{(q^2-m^2)((p+q)^2-m^2)} + 2\int\frac{q^\mu d^4q}{(q^2-m^2)((p+q)^2-m^2)}\right].\tag{16}$$

From direct calculations it results that contribution of this diagram is also zero. Using the Veltman's functions definition:

$$B_0(p^2; m_1, m_2) = \frac{1}{i\pi^2}\int\frac{dq}{(q^2-m_1^2)((p+q)^2-m_2^2)},\tag{17}$$

$$B^\mu(p^2; m_1, m_2) = \frac{1}{i\pi^2}\int\frac{q^\mu d^4q}{(q^2-m_1^2)((p+q)^2-m_2^2)}\tag{18}$$

$$= \frac{p^\mu}{2p^2}\left[-A_0(m_1)+A_0(m_2)-(p^2+m_1^2-m_2^2)B_0(p^2; m_1, m_2)\right],\tag{19}$$

we have found:

$$\Lambda^{\mu} = C\left[p^{\mu}B_0(p^2; m, m) + 2B^{\mu}(p^2; m, m)\right] = C\left[p^{\mu}B_0(p^2; m, m) - p^{\mu}B_0(p^2; m, m)\right] = 0. \quad (20)$$

Thus, it is necessary to analyze more complex tree diagrams. At last, it can be shown that the tree diagram describing the process $e^- B \to \nu_e W^- B$ contribution is non-zero. This amplitude corresponds to the exchange of scalars —Higgs boson and its partner, $\tilde{\sigma}-$meson (see Figure 3 with virtual $W(p_2)$ which decays to $l\bar{\nu}_l$). Note, there is analogous reaction with the scalar states exchange, $e^- \tilde{\pi}^0 \to \nu_e W^- \tilde{\pi}^0$, whose amplitude is half as it is seen from Lagrangian (11). Its' contribution should be added.

However, in order to consider the complete process of quasielastic electron scattering off DM components with neutrino production, it is necessary to take into account diagrams with an intermediate Z-boson. All contributions to the process $eB \to e\nu_e\bar{n}u_e B$ are shown in Figure 4.

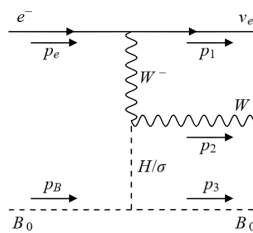**Figure 3.** Quasielastic electron scattering off H-baryon Dark Matter component through intermediate *W*-boson.
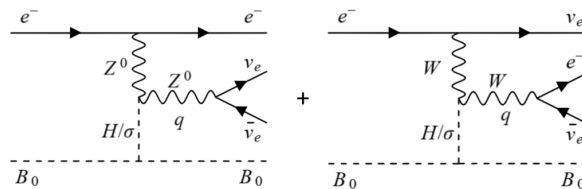

Figure 4. Quasielastic electron scattering off H-baryon through intermediate *W*- and *Z*-bosons.

Here, we omit diagrams with H-quark loops, hhZ and other multi-scalar vertices and so on, which give small contributions to the process considered. In addition, we do not take into account diagrams where the Higgs boson (or $\tilde{\sigma}$-meson) interacts directly with the lepton (electron) current. These amplitudes are suppressed by a small parameter, $\sim m_e/m_{W,Z}$, in comparison with the above diagrams. These small contributions (the amplitudes squared and corresponding interference terms) are no more than 0.01% from total cross section.

4. Numerical Analysis of Leptons Scattering off Hypercolor DM Components

Now, we use the following part of the model Lagrangian:

$$\begin{aligned}
L = \bar{B}^0 B^0 &\left[h(-\lambda_{01}vc_\theta - 2\lambda_{11}us_\theta) + \sigma(\lambda_{01}vc_\theta - 2\lambda_{11}us_\theta)\right] - \\
&\left(g_W m_W W_\mu^+ W_\mu^- + \frac{g_W}{2\cos\theta_W}m_Z Z_\mu Z^\mu\right)(hc_\theta + \sigma s_\theta) + \\
&\frac{-ig_W}{2\sqrt{2}}\bar{\nu}_l\gamma^\mu(1-\gamma_5)lW_\mu^+ - \frac{ig_W}{2\cos\theta_W}\bar{l}\gamma^\mu(C_V - \gamma_5 C_A)lZ_\mu - \\
&\frac{ig_W}{4}\bar{\nu}_l\gamma^\mu(1-\gamma_5)\nu Z_\mu + \text{h.c.,}
\end{aligned} \quad (21)$$

where θ is the angle of Higgs boson, h, and $\tilde{\sigma}-$meson mixing; λ_{01}, λ_{11} are couplings from the Lagrangian (11), v and u are v.e.v's. of h and σ fields. $C_H = c_\theta(\lambda_{01}vc_\theta + 2\lambda_{11}us_\theta)$ and

$C_\sigma = s_\theta(\lambda_{01}vs_\theta - 2\lambda_{11}uc_\theta)$ denote corresponding couplings. Here also $C_V = (4\sin^2\theta_W - 1)/2$, $C_A = -1/2$ are vertex parameters for leptons (electrons). The total amplitude squared has the form:

$$|A|^2 = |A_{WH} + A_{W\sigma} + A_{ZH} + A_{Z\sigma}|^2, \tag{22}$$

where all partial amplitudes are:

$$
\begin{aligned}
A_{WH/\sigma} = \frac{ig^2 m_W C_{H/\sigma}}{2\sqrt{2}\,(2\pi)^{7/2}}\, \Psi^{s_\nu,+}(p_1)\gamma^\nu(1-\gamma_5)\Psi^{s_e,-}(p_e)\times \\
\frac{g_{\mu\nu}-(p_1-p_e)_\mu(p_1-p_e)_\nu/m_W^2}{(p_1-p_e)^2-m_W^2}\frac{g_{\mu\alpha}-(p_2)_\mu(p_2)_\alpha/m_W^2}{(p_2)^2-m_W^2}\frac{\bar\Psi^{s_\nu,+}(k_1)\gamma^\alpha(1-\gamma_5)\Psi^{s_e,-}(k_2)}{(p_3-p_B)^2-m_{H/\sigma}^2},\\
A_{ZH/\sigma} = \frac{ig^2 m_Z C_{H/\sigma}}{4\cos\theta_W\,(2\pi)^{7/2}}\, \Psi^{s_e,+}(k_2)\gamma^\nu(C_V-C_A\gamma_5)\Psi^{s_e,-}(p_e)\times \\
\frac{g_{\mu\nu}-(k_2-p_e)_\mu(k_2-p_e)_\nu/m_Z^2}{(k_2-p_e)^2-m_Z^2}\frac{g_{\mu\alpha}-(p_2)_\mu(p_2)_\alpha/m_Z^2}{(p_2)^2-m_Z^2}\frac{\bar\Psi^{s_\nu,+}(k_1)\gamma^\alpha(1-\gamma_5)\Psi^{s_\nu,-}(p_1)}{(p_3-p_B)^2-m_{H/\sigma}^2}.
\end{aligned}
\tag{23}
$$

Coefficients C_V, C_A were introduced above, p_e, p_B are 4-momenta for incident electron and H-baryon, p_1, k_1 and k_2 are 4-momenta for final neutrinos and electron, correspondingly, and $p_2 = k_1 + k_2$ or $p_2 = k_1 + p_1$ for diagrams with virtual decaying W or Z; further we will neglect of leptons masses. Then, the differential cross section has the standard form:

$$d\sigma = \frac{(2\pi)^2}{V(p)}|A|^2\delta^4(p_e + p_B - p_1 - k_1 - k_2 - p_3)\frac{d\mathbf{p_1}}{2\varepsilon_1}\frac{d\mathbf{k_1}}{2\varepsilon_{k1}}\frac{d\mathbf{k_2}}{2\varepsilon_{k2}}\frac{d\mathbf{p_3}}{2\varepsilon_3}, \tag{24}$$

here ε_i are energies of particles, $V(p)\varepsilon_e\varepsilon_B = \sqrt{(p_e p_B)^2 - m_e^2 m_B^2} = p_e p_B$ is the invariant initial flux. However, we do not calculate cross section for this complex tree process with four final particles exactly. Instead, we use the known method of factorization [44,45] to estimate the total cross section for the process $eB \to e\nu_e\bar\nu_e B$ from convolution integral:

$$
\begin{aligned}
\sigma(ab \to cdik) \approx \sigma(ab \to cd(R(q) \to ik)) = \\
\int_{q_{min}^2}^{q_{max}^2} \sigma(ab \to cdR(q)) \cdot \frac{q\Gamma(R(q) \to ik)dq^2}{\pi|P_R(q)|^2}.
\end{aligned}
\tag{25}
$$

Here, the width of virtual state multiplying by $q = (q^2)^{1/2}$ is $q\Gamma(V(q) \to l\bar\nu_l) = q\Gamma(V(q) \to \nu_l\bar\nu_l) = g^2(q^2)/12\pi$ and $P_R(q) = q^2 - M_R^2 + iM_R\Gamma_{tot}(R)$. The method allows calculating independently both A_{WH} and A_{ZH} squared, and then estimate the interference of these amplitudes. In fact, we consider in this approach some "averaged" process where final electron and neutrinos are produced by different vertices describing the decays $W(p_2) \to l\nu_l$ and $Z(p_2 \to \nu_l\bar\nu_l)$; however, for the massless leptons these vertices coincide, so the method can be applied.

Certainly, in this approach (without using of complex computer programs) we cannot extract an exhausted information on angle and energy distribution of secondary neutrinos or electron. Nevertheless, the total cross section of the reaction can be found with reasonable accuracy. As it is known from numerous applications of the factorization approach [46,47], accuracy of the method is not worse than 1–2%. This is enough for a preliminary analysis of this type of processes, and we can estimate the possibility to detect neutrino producing by cosmic electron scattering at IceCube. Besides, we consider this process in the kinematics when final H-baryon has a small energy, i.e., practically all energy of the incident electron is distributed between three final massless particles (electron and pair of neutrinos). Then, the energies of secondary neutrinos are, approximately, in the interval $\sim(E_e/3$–$E_e)$.

As an example, let us look how to calculate one of the amplitude squared, $|A_{WH}|^2$. The set of independent invariants is as follows:

$$
\begin{aligned}
s &\equiv (p_e + p_B)^2 = (p_1 + p_2 + p_3)^2, \\
s_1 &\equiv (p_1 + p_2)^2 = (p_e + p_B - p_3)^2, \\
s_2 &\equiv (p_2 + p_3)^2 = (p_e + p_B + p_1)^2, \\
t_1 &\equiv (p_e - p_1)^2 = (p_2 + p_3 - p_B)^2, \\
t_2 &\equiv (p_e - p_3)^2 = (p_1 + p_2 - p_e)^2.
\end{aligned}
\tag{26}
$$

Therefore, the contribution of this amplitude squared to the cross section can be written as:

$$
d\sigma = \frac{g^4 m_W^2}{\pi^4 2^{13}(s - m_B^2)} \frac{-t_1 + (s_1 + t_1 - t_2)(s_1 - q^2)/q^2}{\sqrt{-\Delta_4}\,(t_1 - m_W^2)^2} \times \left[\frac{C_H}{t_2 - m_H^2} - \frac{C_\sigma}{t_2 - m_\sigma^2}\right]^2 ds_1 ds_2 dt_1 dt_2, \quad (27)
$$

where the Gram determinant is

$$
\begin{aligned}
\Delta_4 = \Delta_4(p_a, p_b, p_1, p_2) &= \frac{1}{16}
\begin{vmatrix}
2m_a^2 & 2p_a \cdot 2p_b & 2p_a \cdot 2p_1 & 2p_a \cdot 2p_3 \\
2p_a \cdot 2p_b & 2m_b^2 & 2p_b \cdot 2p_1 & 2p_b \cdot 2p_3 \\
2p_a \cdot 2p_1 & 2p_b \cdot 2p_1 & 2m_1^2 & 2p_1 \cdot 2p_3 \\
2p_a \cdot 2p_3 & 2p_b \cdot 2p_3 & 2p_1 \cdot 2p_3 & 2m_2^2
\end{vmatrix} \\
&= \frac{1}{16}
\begin{vmatrix}
2m_a^2 & s - t_1 + m_b^2 & s + s_2 - m_1^2 & s_2 - m_2 + m_3^2 \\
s_2 - t_1 + m_b^2 & 2m_b^2 & s - m_a^2 & m_b^2 + m_3^2 - t_2 \\
s + s_2 - m_1^2 & s - m_a^2 + m_b^2 & 2m_1^2 & s - s_1 + m_3^2 \\
s_2 - m_2^2 + m_3^2 & m_b^2 + m_3^2 - t_2 & s - s_1 + m_3^2 & 2m_2^2.
\end{vmatrix}
\end{aligned}
$$

For fixed s the physical region is defined by inequality

$$
\Delta_4 \leq 0.
$$

Determinant Δ_4 is a polynomial of the second order under s_1:

$$
\Delta_4 = \frac{1}{16}(Ps_1^2 + 2Qs_1 + R) = \frac{P}{16}(s_1 - s_1^+)(s_1 - s_1^-),
$$

where roots $s_1^{\pm}$ are borders of the physical region. Coefficient P is defined by triangle function $\lambda(x, y, z) = (x - y - z)^2 - 4yz$, namely:

$$
P = \lambda(t_1, s_2.m_B^2).
$$

Then, for Q and R we have:

$$
R = 16\Delta_4\Big|_{s_1=0},
$$

$$
4(Q^2 - PR) = 16G(s_2, t_2, t_1, q^2, 0, m_B^2)G(s, t_1, s_2, m_B^2, m_B^2, 0),
$$

$$
Q =
\begin{vmatrix}
2t_1 & t_1 + s_2 - m_B^2 & t_1 - t_2 \\
s_2 + t_1 - m_B^2 & 2s_2 & s_2 - q^2 \\
t_1 - m_B^2 & s_2 - s & 0
\end{vmatrix},
$$

where $G(x, y, z, u, v, w)$ is four-point kinematic function:

$$G(x, y, z, u, v, w) = x^2 y + xy^2 + 2z^2 u + 2v^2 w + xuv + yzw + yuw +$$
$$xzw - xy(z + u + v + w) - zu(x + 2y + w) - vw(x + y + z + u).$$

Now, integration over s_1 is possible and it leads to:

$$I_1 = \int_{s_1^-}^{s_1^+} \frac{As_1^2 + Bs_1 + C}{\sqrt{-Ps_1^2 - 2Qs_1 - R}} ds_1 = \frac{\pi C}{P^{1/2}} - \frac{\pi BQ}{P^{3/2}} + A \left[\frac{5}{2}(Q^2 - PR) + PR \right] \frac{\pi}{P^{5/2}}$$

This part of the cross section takes the form:

$$d\sigma = C \int \frac{I_1(t_1, t_2, s_2)}{(t_1 - m_W^2)^2} \left[\frac{C_H}{t_2 - m_H^2} - \frac{C_\sigma}{t_2 - m_\sigma^2} \right]^2 dt_1 ds_2 dt_2 \tag{28}$$

As P depends on t_1, s_2, an integration over t_2 is simple:

$$\int_{t_1^-}^{t_2^+} \frac{D_1 t_2^2 + E_1 t_2 + F_1}{A_1 t_2^2 + B_1 t_2 + C_1} dt_2,$$

and we get a compact expression for this contribution to the cross section:

$$d\sigma = C \int \frac{I_2(t_1, s_2)}{(t_1 - m_W^2)^2} dt_1 ds_2, \tag{29}$$

where

$$I_2 = C_H^2 I_H + C_\sigma^2 I_\sigma + 2 C_H C_\sigma I_{H\sigma},$$

Here I_H, I_σ and $I_{H\sigma}$ are the following integrals:

$$I_H = \left[D_1(t_2 - m_H^2) + 2(E_1 + 2m_H^2 D_1) \ln(t_2 - m_H^2) - (F_1 + m_H^4 D_1 + m_H^2 E_1) \frac{1}{t_2 - m_H^2} \right] \Big|_{t_2^-}^{t_2^+}, \tag{30}$$

and $I_\sigma = I_H(m_H \rightarrow m_\sigma)$. We also get contribution for interference of h and $\tilde{\sigma}$ diagrams in amplitude A_{WH} squared:

$$I_{H\sigma} = \frac{D_1}{2}(t_2^+ - t_2^-)(m_H^2 + m_\sigma^2) \quad + \frac{1}{2} \left(E_1 - D_1(m_H^2 + m_\sigma^2) \right)$$
$$\times \ln \left[\left(t_2 - \frac{1}{2}(m_H^2 + m_\sigma^2) \right)^2 + \frac{1}{4}(m_\sigma^2 - m_H^2)^2 \right] \Big|_{t_2^-}^{t_2^+} \tag{31}$$
$$+ \frac{2F_1 + 2m_H^2 m_\sigma^2 D_1 + E_1(m_H^2 + m_\sigma^2)}{m_\sigma^2 - m_H^2} \arctan \left[\frac{t_2 - m_\sigma^2 - m_H^2}{m_\sigma^2 - m_H^2} \right] \Big|_{t_2^-}^{t_2^+}.$$

The above limits are:

$$t_2^\pm = 2m_B^2 - \frac{1}{2s_2} \left[(s_2 + m_B^2 - t_1)(s_2 + m_B^2 - q^2) \mp \lambda^{1/2}(s_2, m_B^2, t_1) \lambda^{1/2}(s_2, q^2, m_B^2) \right].$$

For the total amplitude squared (22) separate terms are considered analogously. Because these expressions are very cumbersome, they were analyzed numerically. In calculations we use $\sin\theta = 0.05$, $\mu = (1500–2000)$ TeV, and two values of masses of H-baryon: 600 and 1200 GeV. In the model there is a correlation between masses of $m_{\tilde\sigma}$ and $m_{\tilde\pi}$: $m_{\tilde\sigma}^2 \approx 3 \cdot m_{\tilde\pi}^2$. This is an exact equality for zero mixing of Higgs boson and $\tilde\sigma-$meson. Here, we also suppose the splitting between masses of H-baryon and $\tilde\pi^0$ is small, then we can fix approximately the mass of $\tilde\sigma$.

As it is shown (see Figure 5a,b) in the scattering channel with scalar boson exchange, a strong dependence of the cross section on the B-baryon mass is revealed. We present the cross section values for high energy region despite the fact that the cosmic electrons flux noticeably decreases for these energies. The hope is the high-energy neutrinos are detected by IceCube with a larger probability (see below).
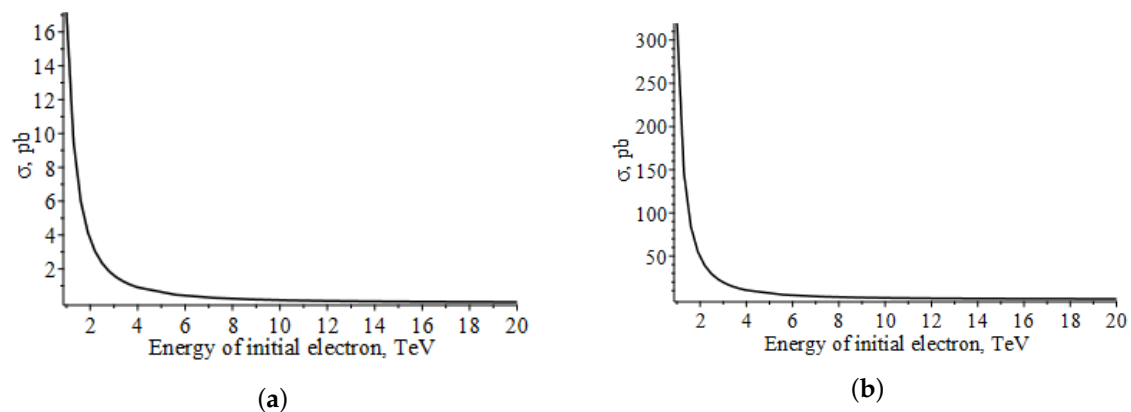

(a)   **(b)**

Figure 5. Total cross section of neutrino production in the laboratory system by quasielastic scattering of cosmic electrons with energies (1–20) TeV off H-baryon Dark Matter component with (**a**) $m_B = 600$ GeV and (**b**) $m_B = 1200$ GeV.

Here, using the factorization method, the channel with secondary electron and two electronic neutrinos already has been separated from channels with other leptons. The presented total cross sections are the sum of contributions from the cosmic ray scattering off both DM components, H-baryons (B and $\bar{B}$) and neutral H-pions, $\tilde\pi^0$. Please note, negative interference of contributions with virtual W- and Z-bosons is numerically important, it decreasing the cross section nearly twice.

As it seems, features of the processes considered are specific for the models where some additional degrees of freedom, arising as pNG-states, interact with the world of ordinary fermion matter through scalars—Higgs-boson and/or its partners (or via H-quark and H-pion loops). As a result, the cross section is amplified due to strong vertices of scalar interaction with fermions ($ht\bar{t}$, for example) and vector or scalar bosons. Just this situation is realized in H-color model where H-baryon component of the hidden mass prefer to interact directly with scalars not with vector bosons. We also found that the cross section strongly depends on the H-particle mass.

5. Can the Signals of Secondary Neutrinos Be Observed?

To estimate the number of neutrino events which would be observed by IceCube, it should be to integrate the cross section $\sigma_{tot}(E_e)$ multiplied by differential flux of cosmic electrons over their energies (see Refs. [20,48–50] for details of the procedure). This flux of electron component of cosmic rays is known with a sufficient accuracy and is a power function of electron energy with some detail of this dependence in various energy regions [51–54].

Knowing only total cross sections of neutrino production, we can evaluate the fluxes of neutrinos produced by scattering of electrons with energies in some intervals $\Delta_E = E_{e,2} - E_{e,1}$ as:

$$N(\Delta_E) = r_\odot \rho_\odot \bar{J} \frac{1}{M_{DM}} \int_{E_{e,1}}^{E_{e,2}} dE_e \frac{d\Phi}{dE_e} \cdot \sigma(E_e). \tag{32}$$

Here, the DM density is $\rho_\odot = 0.3 \text{ GeV/cm}^3$ at the Sun location and $r_\odot = 8.33 \text{ kpc}$. The energy spectrum of cosmic electrons can be approximated as $d\Phi/dE_e = k_e(E/GeV)^{-a}$ with $a = (2.7-3.1)$ [51,53,55] and $k_e \approx 0.03 \text{ GeV}^{-1}\text{cm}^{-2}\text{s}^{-1}\text{sr}^{-1}$. We use this form of the spectrum for electron energies up to $\sim(10-20) \text{ TeV}$. A noticeable increasing of the cosmic ray flux near the Galaxy Center (GC), can be simulated by an additional factor $f(r(s,\theta)) = \exp(r_\odot - r)/r_0$ (see e.g., Ref. [49] and references therein).

Astrophysical factor $\bar{J}$ is defined as:

$$\bar{J} = \frac{2\pi}{\Delta\Omega} \frac{1}{r_\odot \rho_\odot} \int_{\Delta\Omega} d\theta \sin\theta \int_0^{2r_\odot} ds \rho(r(s,\theta)) \cdot f(r(s,\theta)), \tag{33}$$

where $r(s,\theta) = (s^2 + r_\odot^2 - 2s * r_\odot * \cos\theta)^{1/2}$ is the coordinate with center in GC, $\Delta\Omega$ is the angle of observation from the Earth, and we focus on the direction towards the GC. An angular region of $\theta = 1^0$ around the GC corresponds to $\Delta\Omega \approx 10^{-3}$. For the model of the DM distribution, spherically symmetric Einasto profile is used:

$$\rho(r(s,\theta)) = \rho_s exp\left[-\frac{2}{\alpha} \left(\frac{r}{r_s}\right)^\alpha - 1 \right]. \tag{34}$$

Parameters of the standard profile—typical scale radius, scale density and the slope of the profile—are the following:

$$r_s = 35.24 \text{ kpc}, \quad \rho_s = 0.021 \text{ GeV/cm}^3, \quad \alpha = 0.17.$$

The so-called modified Einasto profile with $\alpha = 0.11$ was derived from numerical simulations including the baryons contribution [3,56], this profile is somewhat steeper near the GC.

In Table 2 the integral neutrino fluxes producing by cosmic electrons with energies from intervals Δ_E are presented for the case of modified Einasto profile with an account of the amplifying factor $f(r)$. These fluxes depend on the energies of initial electron drastically.

Table 2. Fluxes of secondary neutrinos for different interval of incident electron energies and two possible values of H-hadron mass, $\alpha = 0.11$.

Interval of Initial Electron Energies, TeV	Neutrino Flux, $m_B = 0.6$ TeV	Neutrino Flux, $m_B = 1.2$ TeV
1–2	3.3×10^{-21}	2.7×10^{-20}
2–4	2.2×10^{-22}	1.4×10^{-21}
4–8	1.8×10^{-23}	1.0×10^{-22}
8–12	1.1×10^{-24}	0.6×10^{-23}
12–20	2.7×10^{-25}	1.4×10^{-24}

Here, the astrophysics neutrino flux, N, is measured in $\text{cm}^{-2}\text{sr}^{-1}\text{s}^{-1}$. Obviously, the fluxes calculated are very small in comparison with expected atmospheric neutrino fluxes which are $\sim 10^{-10}$–$10^{-9} \text{ cm}^{-2}\text{sr}^{-1}\text{s}^{-1}$ at neutrino energies ≥ 1 TeV [57–59]. These atmospheric neutrinos produced by decays of mesons and baryons generating by interaction of high-energy cosmic rays with nuclei in atmosphere. It is practically impossible to separate the neutrino signals generated by scattering reactions from this constant and large background. Such small values of galactic neutrino

fluxes mainly result from the low intensity of cosmic electrons flux which steeply decreases at energies $E_e \geq 1$ TeV.

The number of neutrinos landing on the IceCube [59–61] surface area (which is ≈ 1 km^2) during the year is estimated as very small $N_\nu \approx 10^0$ for neutrino with energies in the interval (1–2) TeV and $m_B = 1200$ GeV. This estimation slightly depends on other DM profile details, all known profiles of the DM nearly coincide at the distances ≥ 1 kpc from the GC [3].

The probability of registration at IceCube neutrinos with these energies is also very small. Namely, the probability is defined by IceCube effective area [59,62–64]), A_{eff} is an equivalent area for which all neutrino from a neutrino flux impinging on the Earth would be detected. The probability of identifying an observed cascade signal with the neutrino event is found as $P(E_\nu) \approx A_{eff}(E_\nu)/A$, where A is the total detector area. Having data on the effective area for registration of electronic neutrino [64–66], we get: $A_{eff} \approx 10^{-2}$ m^2 for $E_{\nu_e} \approx 1$ TeV, the effective area slightly increases up to $\approx (10^{-1}$–$10^0)$ m^2 for energies $E_\nu \approx (2$–$20)$ TeV [59,64–66]. For total IceTop area is $A = 10^6$ m^2, we find a small probability to detect events with ν_e for the processes considered: for neutrino energies from 1 to 20 TeV we get $P = 10^{-8}$–10^{-5}.

Thus, from the pessimistic point of view, the processes analyzed do not contribute significantly to the total flux of neutrinos from Galaxy sources. However, consideration of this type of reactions is important because it arises some type of amplitudes amplified due to scalar exchanges channel.

6. Discussion and Conclusions

In this work, analysis of high-energy electrons scattering off the DM components was carried out in the minimal two-H-color model. A cross section of this process was calculated in a quasielastic kinematics with the using of the factorization method. For this process, which is described by four diagrams (excluding an additional small contributions), the total cross section was calculated approximately with an accuracy $\leq 3\%$. In the factorization scheme we cannot consider distributions of final particles on energies and angles, it is possible to estimate only the secondary neutrino flux in dependence on incident electron energy.

An important feature of this analysis is the study of the scattering channel with virtual scalar states, Higgs boson and its partner, $\tilde{\sigma}-$boson. An amplifying of this channel of the reaction is caused by vertex of scalar interaction with the gauge bosons. A strong dependence of the cross section value on the DM component mass was also found; it can be important for the analysis of other possible signals from the hypercolor DM. This significant increasing of cross sections with the H-baryon mass can give some constrains for the DM mass from comparison with astrophysics data on photon and/or lepton fluxes which are generated by processes with the DM participation.

Together with the cross sections, we calculate fluxes of secondary neutrinos depending on incident electron energies. At IceCube the number and intensity of cascades (i.e., power of induced Cherenkov's emission) producing by high-energy neutrinos, strongly depend on energies of landing neutrinos and their fluxes. Probability of neutrino detection was estimated with the known effective areas of IceCUbe for different energies of neutrino. It is shown that the secondary neutrino fluxes and, correspondingly, the predicted number of neutrino events originated by these reactions and for the used set of the model parameters, is too small to be detected.

Despite of the smallness of neutrino events number in the reaction considered, it would be reasonable to study other processes of high-energy particles scattering off the DM:

- creation of additional neutrino pairs, $\nu_l B(\tilde{\pi}) \to \nu_l \nu_{l'} \bar{\nu}_{l'} B(\tilde{\pi})$,
- creation of $l^+ l^-$−pairs, $\nu_l B(\tilde{\pi}) \to \nu_l l^+ l^- B(\tilde{\pi})$,
- reaction $e^- B(\tilde{\pi}) \to e^- l^+ l^- B(\tilde{\pi})$.

Cross sections for these processes can be amplified when high-energy cosmic rays are scattered by the DM inhomogeneities, so-called clumps [67–71]. In these regions the DM density can increase sufficiently resulting in increasing of secondary leptons fluxes. The number of neutrino events will

also grow due to its proportionality to the DM density value. Note, the scattering of initial neutrino off the DM with creation of three secondary neutrinos can be interesting for the study of neutrino flux from the Sun [72].

The flux of secondaries strongly depends not only on the DM clump density but also on the clump localization in the Galaxy, i.e., on the clump angular size and distance from it. As the result, the flux can be enlarged up to ten times or even more. If, for example, such an increase were observed and, in addition, this effect was unambiguously correlated with a certain direction or an object in the Galaxy, this intensive and regular signal could indicate the existence of some type of the DM inhomogeneity.

Electrons are only a small part, $\sim 10^{-3}$, of density of cosmic ray flux, so inelastic interaction of high-energy protons with the hidden mass particles can be more informative about the DM structure and distribution. Namely, these are inclusive reactions: $p^+ B(\tilde{\pi}) \to X l \nu_l B(\tilde{\pi})$, $p^+ B(\tilde{\pi}) \to X \nu_l \bar{\nu}_l B(\tilde{\pi})$ and $p^+ B(\tilde{\pi}) \to l^+ l^- B(\tilde{\pi})$. Due to quark level subprocess, $uB \to dW^+ B$, there occurs a channel with virtual boson decay $W^+ \to e^+ \nu_e$. It would be a source of extra positrons producing by cosmic rays. Certainly, to get a noticeable amount of positrons with energies in the interval 200–500 GeV it should be a large flux of protons with energies near ~ 1 TeV. However, it is at these energies the proton flux is large, so inclusive inelastic reactions with cosmic protons can generate an additional positrons in the spectrum of leptons. Quark level process $dB \to uW^- B$ following by decay $W^- \to e^- \bar{\nu}_e$ also occurs, but it has a nearly twice smaller cross section. Certainly, in this inclusive processes there arise hadron jets with the decaying mesons producing several muons, neutrino, photons, and electron-positron pairs. Nevertheless they also create some quantity of extra positrons, as it is seen. This process is interesting and should be analyzed supposing an existence of some dense DM target near the Earth.

Quasielastic scattering of high-energy photons off the hidden mass particles is possible in reactions such as $\gamma B(\tilde{\pi}^0) \to W^+ W^- B(\tilde{\pi}^0)$, $\gamma B(\tilde{\pi}^0) \to \bar{t} t B(\tilde{\pi}^0)$ with intermediate scalar bosons. In this case, secondary particles are generated in $W-$boson and/or $t-$quark decays.

At high energies, inelastic reactions with the "exciting" of higher states of the pNG H-hadrons can also occur. There can arise non-stable charged di-H-quarks, charged H-pions and other higher H-hadrons (see Table 1 above). These states will eventually decay to neutral stable DM particles producing photons, leptons and standard light mesons in jets of heavy H-hadrons. To analyze these reactions in detail, we should know (or suppose) the spectrum of masses of higher H-hadrons, possible channels and widths of their decays, i.e., the "zoo" of H-particles should be carefully investigated. At this time, consideration of these processes is beyond the scope of this paper.

Thus, the analysis fulfilled allows considering interactions of high-energy cosmic rays with the hidden mass particles as an extra instrument of testing of their properties from indirect signals. In particular, it should be interesting for the scenarios where the DM candidates interact with ordinary leptons and/or quarks mainly through scalar boson exchanges. In this case, the cross section can be noticeably enlarged, so the analysis of masses, charges, angular and energy distributions of secondary particles will be more effective. These processes can be useful additional source of information on the structure of hidden mass and its space distribution.

The suggested H-color model has a rich phenomenolgy allowing formulating several new tasks, such as the studying of heavy stable charged H-mesons in the framework of $SU(6) \to Sp(6)$ symmetry, analysis of the hypercolor vacuum stability, deep-inelastic processes with the H-color pNG-states exciting and so on. The studying of possible astrophysics signals from processes with the H-particles participation is important for comparison of signals generated by different scenarios of physics beyond the SM.

References

1. Khlopov, M.Y. Introduction to the special issue on indirect dark matter searches. *Int. J. Mod. Phys. A* **2014**, *29*, 1443002. [CrossRef]
2. Cirelli, M. Indirect Searches for Dark Matter: A status review. *Pramana* **2012**, *79*, 1021. [CrossRef]
3. Cirelli, M. Dark Matter Indirect searches: Phenomenological and theoretical aspects. *J. Phys. Conf. Ser.* **2013**, *447*, 012006. [CrossRef]
4. Roszkowski, L.; Sessolo, E.M.; Trojanowski, S. WIMP dark matter candidates and searches—Current status and future prospects. *Rept. Prog. Phys.* **2018**, *81*, 066201. [CrossRef]
5. Gaskins, J.M. A review of indirect searches for particle dark matter. *Contemp. Phys.* **2016**, *57*, 496–525. [CrossRef]
6. Arcadi, G.; Dutra, M.; Ghosh, P.; Lindner, M.; Mambrini, Y.; Pierre, M.; Profumo, D.; Queiroz, F.S. The waning of the WIMP? A review of models, searches, and constraints. *Eur. Phys. J. C* **2018**, *78*, 203. [CrossRef]
7. Belotsky, K.M.; Esipova, E.A.; Kamaletdinov, A.K.; Shlepkina, E.S.; Solovyov, M.L. Indirect effects of dark matter. *IJMPD* **2019**, *28*, 1941011. [CrossRef]
8. Berezinsky, V.S.; Dokuchaev, V.I.; Eroshenko, Y.N. Small-scale clumps of dark matter. *Physics-Uspekhi* **2014**, *57*, 1–36. [CrossRef]
9. Pasechnik, R.; Beylin, V.; Kuksa, V.; Vereshkov, G. Chiral-symmetric technicolor with standard model Higgs boson. *Phys. Rev. D.* **2013**, *88*, 075009. [CrossRef]
10. Beylin, V.; Kuksa, V.; Vereshkov, G. Model of vectorlike technicolor. *Phys. Part. Nucl. Lett.* **2016**, *13*, 19–25. [CrossRef]
11. Pasechnik, R.; Beylin, V.; Kuksa, V.; Vereshkov, G. Vectorlike technineutron Dark Matter: Is a QCD-type Technicolor ruled out by XENON100? *Eur. Phys. J. C.* **2014** *74*, 2728. [CrossRef]
12. Kilic, C.; Okui, T.; Sundrum, R. Vector-like Confinement at the LHC. *JHEP* **2010**, *018*, 1093. [CrossRef]
13. Ryttov, T.A.; Sannino, F. Ultra Minimal Technicolor and its Dark Matter TIMP. *Phys. Rev. D.* **2008**, *78*, 115010. [CrossRef]
14. Foadi, R.; Frandsen M.T.; Sannino, F. Technicolor dark matter. *Phys. Rev. D* **2009**, *80*, 037702. [CrossRef]
15. Frandsen, M.T.; Sannino, F. Isotriplet technicolor interacting massive particle as dark matter. *Phys. Rev. D* **2010**, *81*, 097704. [CrossRef]
16. Hambye, T. Hidden vector dark matter. *JHEP* **2009**, *1*, 028. [CrossRef]
17. Beylin, V.; Bezuglov, M.; Kuksa, V.; Volchanskiy, N. An analysis of a minimal vector-like extension of the Standard Model. *Adv. High Energy Phys.* **2017**, *2017*, 1765340. [CrossRef]
18. Cirelli, M.; Fornengo, N.; Strumia, A. Minimal dark matter. *Nucl. Phys. B* **2006**, *753*, 178. [CrossRef]
19. Beylin V.; Khlopov M.Y.; Kuksa V.; Volchanskiy N. Hadronic and hadron-like physics of dark matter. *Symmetry* **2019**, *11*, 587. [CrossRef]
20. Beylin, V.; Bezuglov, M.; Kuksa, V.; Tretiakov, E.; Yagozinskaya, A. On the scattering of a high-energy cosmic ray electrons off the dark matter. *Int. J. Mod. Phys. A* **2019**, *6*, 34. [CrossRef]
21. Beylin, V.; Bezuglov, M.; Tretiakov, E. Signals of Dark Matter in hypercolor vectorlike extension of the SM. *Eur. Phys. J. Web Conf.* **2019**, *222*, 04002. [CrossRef]
22. Weinberg, S. Implication of Dynamical Symmetry Breaking. *Phys. Rev. D* **1976**, *13*, 974996. [CrossRef]
23. Susskind, L. Dynamics of Spontaneous Symmetry Breaking in the Weinberg-Salam Theory. *Phys. Rev. D* **1979**, *20*, 2619–2625. [CrossRef]
24. Appelquist, T. Technicolor and fermion mass enhancement. In *Research Directions for the Decade: Proceedings of the 1990 Summer Study on High Energy Physics*; World Scientific: River Edge, NJ, USA, 1990; pp. 44–49.
25. Farhi, E.; Susskind, L. Technicolor. *Phys. Rep.* **1981**, *74*, 277. [CrossRef]
26. Gell-Mann, M.; Lévy, M. The axial vector current in beta decay. *Nuovo Cim.* **1960**, *16*, 705–726. [CrossRef]
27. Nambu, Y.; Jona-Lasinio, G. Dynamical Model of Elementary Particles Based on an Analogy with Superconductivity. *Phys. Rev.* **1961**, *122*, 345. [CrossRef]

28.　Weinberg, S. A Model of Leptons. *Phys. Rev. Lett.* **1967**, *19*, 1264. [CrossRef]

29.　Fariborz, A.H.; Park, N.W.; Schechter, J.; Naeem Shahid, M. Gauged linear sigma model and pion-pion scattering. *Phys. Rev. D* **2009**, *80*, 113001. [CrossRef]

30.　Pasechnik, R.; Beylin, V.; Kuksa, V.; Vereshkov, G. Composite scalar Dark Matter from vector-like SU(2) confinement. *Int. J. Mod. Phys. A* **2016**, *31*, 1650036. [CrossRef]

31.　Volchanskiy, N.; Kuksa, V.; Beylin, V. Models of hypercolor based on symplectic gauge group with three heavy vectorlike hyperquarks. *Int. J. Mod. Phys. D* **2019**, *28*, 13. [CrossRef]

32.　Bai, Y.; Hill, R.J. Weakly Interacting Stable Pions. *Phys. Rev. D* **2010**, *82*, 111701. [CrossRef]

33.　Antipin, O.; Redi, M.; Strumia, A.; Vigiani, E. Accidental Composite Dark Matter. *JHEP* **2015**, *039*, 1164. [CrossRef]

34.　Cacciapaglia, G.; Sannino, F. Fundamental Composite (Goldstone) Higgs Dynamics. *JHEP* **2014**, *1404*, 111. [CrossRef]

35.　Bennett, E.; Hong, D.K.; Lee, J.-W.; David Lin, C.-J.; Lucini, B.; Piai, M.; Vadacchino, D. Meson spectrum of Sp(4) lattice gauge theory with two fundamental Dirac fermions. *arXiv* **2019**, arXiv:1911.00437.

36.　Bennett, E.; Hong, D.K.; Lee, J.-W.; David Lin C.-J.; Lucini, B.; Piai, M.; Vadacchino, D. Sp(4) gauge theories on the lattice: Nf=2 dynamical fundamental fermions. *JHEP* **2019**, *53*, 12. [CrossRef]

37.　Beylin, V.; Bezuglov, M.; Kuksa, V. Analysis of scalar dark matter in a minimal vectorlike standard model extension. *Int. J. Mod. Phys. A* **2017**, *32*, 1750042. [CrossRef]

38.　Holdom, B. A dynamical origin for the top mass. *Phys.Lett. B* **1994**, *336*, 85–90. [CrossRef]

39.　Gudnason, S.B.; Kouvaris, C.; Sannino, F. Dark Matter from New Technicolor theories. *Phys. Rev. D* **2006**, *74*, 095008. [CrossRef]

40.　Khlopov, M.Y.; Couvaris, S. Strong interative massive particles from a strong coupled theory. *Phys. Rev. D* **2008**, *77*, 065002. [CrossRef]

41.　Khlopov, M.Y.; Couvaris, S. Composite dark matter from a model with composite Higgs boson. *Phys. Rev. D* **2008**, *78*, 065040. [CrossRef]

42.　Belotsky, K.; Khlopov, M.; Kouvaris, C.; Laletin, M. High Energy Positrons and Gamma Radiation from Decaying Constituents of a two-component Dark Atom Model. *IJMPD* **2015**, *24*, 1545004. [CrossRef]

43.　Doff, A.; Natale, A.A. Technicolor models with coupled systems of Schwinger-Dyson equations. *Phys. Rev. D* **2019**, *99*, 055026. [CrossRef]

44.　Kuksa, V.I. The convolution formula for a decay rate. *Phys. Lett. B* **2006** *633*, 545–549. [CrossRef]

45.　Kuksa, V.I.; Volchanskiy, N.I. Factorization in the model of unstable particles with continuous masses. *Cent. Eur. J. Phys.* **2013**, *11*, 182–194. [CrossRef]

46.　Kuksa, V.I.; Pasechnik, R.S. Near-threshold Z-pair production in the model of unstable particles with a smeared mass. *IJMPA* **2008**, *23*, 4125–4132. [CrossRef]

47.　Pasechnik, R.; Kuksa, V. Finite-width effects in the near-threshold ZZZ and ZWW production at ILC. *Mod. Phys. Lett. A* **2011**, *26*, 1075. [CrossRef]

48.　Gorchtein, M.; Profumo, S.; Ubaldi, L. Probing Dark Matter with AGN Jets. *Phys. Rev. D* **2010**, *82*, 083514. [CrossRef]

49.　Profumo, S.; Ubaldi, L. Cosmic Ray-Dark Matter Scattering: a New Signature of (Asymmetric) Dark Matter in the Gamma Ray Sky. *JCAP* **2011**, *020*, 1108. [CrossRef]

50.　Gorchtein, M.; Profumo, S.; Ubaldi, L. Gamma rays from cosmic-ray proton scattering in AGN jets: The intra-cluster gas vastly outshines dark matter. *JCAP* **2013**, *2013*, 012.

51.　Aharonian, F.; Akhperjanian, A.; Barres de Almeida, U.; Bazer-Bachi, A.; Becherini, Y.; Behera, B.; Benbow, W.; Bernlohr, K.; Boisson, C.; Bochow, A.; et al. The energy spectrum of cosmic-ray electrons at TeV energies. *Phys. Rev. Lett.* **2008**, *26*. [CrossRef]

52.　Kachelries, M.; Semikoz, D.V. Cosmic Ray Models. *Nucl. Phys.* **2019**, *109*, 103710. [CrossRef]

53.　Lipari, P. The spectral shapes of the fluxes of electrons and positrons and the average residence time of cosmic rays in the Galaxy. *Phys. Rev. D* **2019**, *99*, 043005. [CrossRef]

54.　Archer, A.; Benbow, W.; Bird, R.; Brose, R.; Buchovecky, M.; Buckley, J.H.; Bugaev, V.; Connolly, M.P.; Cui,W.; Feng, Q.; et al. Measurement of Cosmic-ray Electrons at TeV energies. *Phys. Rev. D* **2018**, *6*, 062004. [CrossRef]

55. Adriani, O.; Akaike, Y.; Asano, K.; Asaoka, Y.; Bagliesi, M.G.; Bigongiari, G.; Binns, W.R.; Bonechi, S.; Bongi, M.; Brogi, P.; et al. Energy Spectrum of Cosmic-Ray Electron and Positron from 10 GeV to 3 TeV Observed with the Calorimetric Electron Telescope on the International Space Station. *Phys. Rev. Lett.* **2017** , *119*, 181101. [CrossRef] [PubMed]

56. Dutton, A.; Maccio, A.V. Cold dark matter haloes in the Planck era: Evolution of structural parameters for Einasto and NFW profiles. *Mon. Not. R. Astron. Soc.* **2014**, *441*, 4. [CrossRef]

57. Richard, E.; Okumura, K.; Abe, K.; Haga, Y.; Hayato, Y.; Ikeda, M.; Iyogi, R.; Kameda, J.; Kishimoto, Y.; Miura, M.; et al. Measurements of the atmospheric neutrino flux by Super-Kamiokande: Energy spectra, geomagnetic effects, and solar modulation. *Phys. Rev. D* **2016**, *94*, 052001. [CrossRef]

58. Kochanov, A.A.; Morozova, A.D.; Sinegovskaya, T.S.; Sinegovskiy, S.I. Behaviour of the high-energy neutrino flux in the Earth's atmosphere. *Sol.-Terr. Phys.* **2015**, *1*, 4.

59. Ahlers, M.; Helbing, K.; de los Heros, C.P. Probing particle physics with IceCube. *Eur. Phys. J. C* **2018**, *78*, 924. [CrossRef]

60. Ishihara, A. Extremely high energy neutrinos in six years of IceCube data. *J. Phys. Conf. Ser.* **2016**, *718*, 062027. [CrossRef]

61. Aartsen, M.G.; Abbasi, R.; Abdou, Y.; Ackermann, M.; Adams, J.; Aguilar, J.A.; Ahlers, M.; Altmann, D.; Auffenberg, J.; Bai, X.; et al. Evidence for High-Energy Extraterrestrial Neutrinos at the IceCube Detector. *Science* **2013**, *342*, 1242856.

62. Chiarusi, T.; Spurio, M. High-Energy Astrophysics with Neutrino Telescopes. *Eur. Phys. J. C* **2010**, *65*, 649–701. [CrossRef]

63. Karle, A. IceCube. In Proceedings of the 31th ICRC2009, Lodz, Poland, 7–15 July 2009; p. 1339.

64. Niederhausen, H.; Xu, Y. High Energy Astrophysical Neutrino Flux Measurement Using Neutrino-induced Cascades Observed in 4 Years of IceCube Data. In Proceedings of the ICRC2017, Busan, Korea, 12–20 July 2017; p. 968. [CrossRef]

65. Brayer, L.; Casier, M.; Golup, G.; van Eindhoven, N. The IceCube Neutrino Observatory—Contributions to ICRC 2015 Part I: Point Source Searches. In Proceedings of the ICRC2015, The Hague, The Netherlands, 30 July–6 August 2015; p. 1048. [arXiv:1510.05222]

66. Aartsen, M.G.; Abraham, K.; Ackermann, M.; Adams, J.; Aguilar, J.A.; Ahlers, M.; Ahrens, M.; Altmann, D.; Anderson, T.; Ansseau, I.; et al. The IceCube Neutrino Observatory Contributions to ICRC 2015 Part II: Atmospheric and Astrophysical Diffuse Neutrino Searches of All Flavors. *arXiv* **2015**, arXiv:1510.05222.

67. Berezinsky, V.; Dokuchaev, V.; Eroshenko, Y. Small-scale clumps in the galactic halo and dark matter annihilation. *Phys. Rev. D* **2003**, *68*, 103003. [CrossRef]

68. Berezinsky, V.; Dokuchaev, V.; Eroshenko, Y. Remnants of dark matter clumps. *Phys. Rev. D* **2008**, *77*, 083519. [CrossRef]

69. Berezinsky, V.; Dokuchaev, V.; Eroshenko, Y. Formation and internal structure of superdense dark matter clumps and ultracompact minihaloes. *JCAP* **2013**, *59*, 1311. [CrossRef]

70. Belotsky, K.; Kirillov, A.; Khlopov, M. Gamma-ray evidences of the dark matter clumps. *Grav. Cosmol.* **2014**, *20*, 47. [CrossRef]

71. Tasitsiomi, A.; Olinto, A.V. Detectability of neutralino clumps via atmospheric Cherenkov telescopes. *Phys. Rev. D* **2002**, *66*, 083006. [CrossRef]

72. Fornengo, N.; Masiero, A.; Queiroz, F.S.; Yaguna, C.E. On the role of neutrinos telescopes in the search for Dark Matter annihilations in the Sun. *JCAP* **2017**, *2017*, 012. [CrossRef]